

Search for sub-electronvolt solar axions using coherent conversion of axions into photons in magnetic field and gas helium

Yoshizumi Inoue^{a,e,*}, Toshio Namba^c, Shigetaka Moriyama^c,
Makoto Minowa^{b,e}, Yuko Takasu^b,
Takashi Horiuchi^b, and Akira Yamamoto^d

^a*International Center for Elementary Particle Physics, University of Tokyo,
7-3-1 Hongo, Bunkyo-ku, Tokyo 113-0033, Japan*

^b*Department of Physics, School of Science, University of Tokyo, 7-3-1 Hongo,
Bunkyo-ku, Tokyo 113-0033, Japan*

^c*Kamioka Observatory, Institute for Cosmic Ray Research, University of Tokyo,
Kamioka-cho, Yoshiki-gun, Gifu 506-1205, Japan*

^d*High Energy Accelerator Research Organization (KEK), 1-1 Oho, Tsukuba,
Ibaraki 305-0801, Japan*

^e*Research Center for the Early Universe (RESCEU), School of Science, University
of Tokyo, 7-3-1 Hongo, Bunkyo-ku, Tokyo 113-0033, Japan*

Abstract

A search for solar axions has been performed using an axion helioscope which is equipped with a 2.3 m-long 4 T superconducting magnet, PIN-photodiode X-ray detectors, and a telescope mount mechanism to track the sun. In addition, a gas container to hold dispersion-matching gas has been developed and a mass region up to $m_a = 0.27$ eV was newly explored. From the absence of any evidence, analysis sets a limit on axion-photon coupling constant to be $g_{a\gamma\gamma} < 6.8\text{--}10.9 \times 10^{-10} \text{GeV}^{-1}$ for the axion mass of $0.05 < m_a < 0.27$ eV at 95% confidence level, which is more stringent than the limit inferred from the solar-age consideration. This result gives currently the most stringent observational limit on the existence of solar axions in this mass region.

Key words: solar axion, helioscope, PIN photodiode, superconducting magnet
PACS: 14.80.Mz, 07.85.Fv, 96.60.Jw

* Corresponding author

Email address: berota@icepp.s.u-tokyo.ac.jp (Yoshizumi Inoue).

1 Introduction

Quantum chromodynamics (QCD) is widely accepted as the theory of strong interactions, but has one flaw called the strong CP problem, i.e., the neutron electric dipole moment is $O(10^9)$ times smaller than expected. The axion is a Nambu–Goldstone boson of the broken Peccei–Quinn (PQ) symmetry which was introduced to solve this problem [1–5]. The expected behavior of an axion is characterized mostly by the scaling factor of the PQ symmetry breaking, f_a , and so its mass, m_a , which is directly related to f_a by $m_a = 6 \times 10^{15}[\text{eV}^2]/f_a$. Laboratory experiments, astrophysical and cosmological considerations have constrained [6–8] the allowed mass region into two. One is at micro- to milli-electronvolts order, where axions can be an ideal dark matter, and the other called ‘hadronic axion window’ is at around one to a few electronvolts, where some hadronic axion models are possible. In the latter region, the sun can be a powerful source of axions and the so-called ‘axion helioscope’ technique may enable us to detect such axions directly [9,10].

The principle of the axion helioscope is illustrated in Fig. 1. Axions would be produced through the Primakoff process in the solar core. The differential flux of solar axions at the Earth is approximated by [10,14]

$$\begin{aligned} d\Phi_a/dE &= 4.02 \times 10^{10} [\text{cm}^{-2}\text{s}^{-1}\text{keV}^{-1}] \\ &\times \left[\frac{g_{a\gamma\gamma}}{10^{-10}\text{GeV}^{-1}} \right]^2 \frac{(E/1\text{keV})^3}{\exp(E/1.103\text{keV}) - 1}, \end{aligned} \quad (1)$$

where $g_{a\gamma\gamma}$ is the axion-photon coupling constant. Their average energy is 4.2 keV reflecting the core temperature of the sun. Then, they would be coherently converted into X-rays through the inverse process in a strong magnetic field at a laboratory. The conversion rate is given by

$$P_{a \rightarrow \gamma} = \frac{g_{a\gamma\gamma}^2}{4} \left| \int_0^L B_{\perp} e^{iqz} dz \right|^2, \quad (2)$$

where z is the coordinate along the incident solar axion, B_{\perp} is the strength of the transverse magnetic field, L is the length of the field along z -axis, $q = |(m_{\gamma}^2 - m_a^2)/2E|$ is the momentum transfer by the virtual photon, and m_{γ} is the effective mass of the photon which equals zero in vacuum.

From 26th till 31st December 1997, the first measurement [11] was performed using an axion helioscope with a dedicated superconducting magnet which we will describe in detail in Section 2 except that the gas container was absent and the conversion region was vacuum. From the absence of an axion signal, an upper limit on the axion-photon coupling is given to be $g_{a\gamma\gamma} < 6.0 \times$

10^{-10}GeV^{-1} (95% CL) for $m_a < 0.03\text{eV}$. However, it was less sensitive to heavier axions, since the momentum transfer, q , becomes non-negligible.

If one can adjust m_γ to m_a , coherence will be restored. This is achieved by filling the conversion region with gas. A photon in the X-ray region acquires a positive effective mass in a medium. In light gas, such as hydrogen or helium, it is well approximated by

$$m_\gamma = \sqrt{\frac{4\pi\alpha N_e}{m_e}}, \quad (3)$$

where α is the fine structure constant, m_e is the electron mass, and N_e is the number density of electrons. We adopted cold helium gas as a dispersion-matching medium. Here, light gas was preferred since it minimizes self absorption by gas. It is worth noting that helium remains at gas state even at 5 K, the operating temperature of our magnet. Since the bore of the magnet is limited in space, the easiest way is to keep the gas at the same temperature as the magnet. Moreover, axions as heavy as a few electronvolts can be reached with helium gas of only about one atmosphere at this temperature.

In this paper, we will present the result of a measurement in which we scanned the mass region up to 0.27 eV.

2 Experimental apparatus

The schematic figure of the axion helioscope is shown in Fig. 2. It is designed to track the sun in order to achieve long exposure time. It consists of a superconducting magnet, X-ray detectors, a gas container, and an altazimuth mounting. In the following paragraphs, we will describe each part in due order.

The superconducting magnet [22] consists of two 2.3-m long race-track shaped coils running parallel with a 20-mm wide gap between them. The magnetic field in the gap is 4 T perpendicular to the helioscope axis. The coils are kept at 5–6 K during operation. In order to make it easy to swing this huge cryogenic apparatus, two devices are engaged. First, the magnet was made cryogen-free by making two Gifford-McMahon refrigerators to cool it directly by conduction. Second, a persistent current switch was equipped. Thanks to this, the magnet can be freed from thick current leads after excitation, and the magnetic field is very stable for a long period of time without supplying current.

The container to hold dispersion-matching gas is inserted in the $20 \times 92\text{mm}^2$ aperture of the magnet. Its body is made of four 2.3-m long 0.8-mm thick

stainless-steel square pipes welded side by side to each other. The entire body is wrapped with 5N high purity aluminium sheet to achieve high uniformity of temperature. The measured thermal conductance between the both ends was $1 \times 10^{-2} \text{W/K}$ at 6 K. One end at the forward side of the container is sealed with welded plugs and is suspended firmly by three Kevlar cords. The opposite side nearer to the X-ray detectors is flanged and fixed to the magnet. At this end of the container, gas is separated from vacuum with an X-ray window manufactured by METOREX which is transparent to X-ray above 2 keV and can hold gas up to 0.3 MPa at liquid helium temperature.

Sixteen PIN photodiodes, Hamamatsu Photonics S3590-06-SPL, are used as the X-ray detectors, whose chip sizes are $11 \times 11 \times 0.5 \text{ mm}^3$ each. The effective area of a photodiode was measured formerly using a pencil-beam X-ray source, and found to be larger than $9 \times 9 \text{ mm}^2$. Each chip is mounted on a Kapton film bonded to an Invar plate with cryogenic compatible adhesive. The X-ray detectors are mounted in a 10-mm thick radiation shielding box made of oxygen-free high conductivity copper (OFHC Cu), which is then surrounded by a lead shield of about 150 mm thick. The copper shield is operated at about 60 K, so that it also functions as a cold finger for the X-ray detectors. Details on the X-ray detector are given in Ref. [12].

The output from each photodiode is fed to a charge sensitive preamplifier whose first-stage FET is at the cryogenic stage near the photodiode chip and the preamplifier outputs are digitized using CAMAC flash analog-to-digital convertors (FADC's), REPIC RPC-081's, at a sampling rate of 10 MHz. The preamplifier outputs are also fed to shaping amplifiers, Clear Pulse CP4026, whose outputs are then discriminated to generate triggers. Thus, waveforms of the sixteen preamplifier outputs are recorded simultaneously over $50 \mu\text{s}$ before and after each trigger to be committed to later off-line analysis. Each detector was calibrated by 5.9-keV Mn X-rays from a ^{55}Fe source installed in front of them. The source is manipulated from the outside and is completely retracted behind the shield during the axion observations.

The entire axion detector is constructed in a vacuum vessel and the vessel is mounted on an altazimuth mount. Its trackable altitude ranges from -28° to $+28^\circ$ and its azimuthal direction is limited only by a limiter which prevents the helioscope from endless rotation. This view corresponds to an exposure time of about a half of a day in observing the sun in Tokyo at $139^\circ 45' 48''$ E and $35^\circ 42' 49''$ N. This is enough for our purpose, since background is measured during the other half of a day. This helioscope mount is driven by two AC servo motors controlled by a computer (PC). The PC also monitors the azimuthal and altitudinal directions of the helioscope regularly by two precision rotary encoders and forms a feedback controlling loop as a whole. The U.S. Naval Observatory Vector Astronomy Subroutines (NOVAS) [13] were used to calculate the solar position. The directional origin was determined

using a theodolite. The altitudinal origin was determined from a spirit level. While the sun is not directly visible from the laboratory in the basement floor, the azimuthal origin was first determined from the observed direction of Polaris (α -UMi) outdoors, and then it was introduced to the laboratory with the theodolite.

Since the effective aperture of the helioscope is narrow, it is crucial to determine its accurate geometry. The axis of the helioscope is defined by two cross hairs at the edge of the vacuum vessel. The position of each part of the helioscope was measured relative to these cross hairs from their exterior using the theodolite when they were installed. The positions of the PIN photodiodes were determined relative to the copper shielding box from a photo image taken prior to the installation. As it is hard to estimate analytically the effect of the geometrical errors as well as the effect of the size of the axion source, we performed a Monte Carlo simulation and found that the overall effective area is larger than 602 mm^2 at 99% confidence level.

3 Measurement and Analysis

From 29th July till 1st September 2000, a measurement employing dispersion-matching gas was performed for ten photon mass settings to scan up to 0.27 eV which is shown in Table 1. The actual gas density was determined using a Yokokawa MU101 precision pressure gauge and two Lakeshore CGR thermistors attached to the gas container, and was calculated based on interpolation of the tables from NIST [23].

Before obtaining energy spectra, each event was categorized into two major groups, the solar observation and the background. Events while the measured direction agreed with the sun are counted as former. When the sun is completely out of the magnet aperture, events are counted as latter. Otherwise events are discarded.

Then, the following bad events are discarded; (a) events containing saturated waveforms, (b) events containing multiple pulses, (c) events containing pulses which are too early or too late compared to their triggers, and (d) events containing pulses whose rise-time is too slow. Cut (a) can be classified into two cases. One is such events where the saturation is caused by a giant pulse, e.g., by cosmic muons. Another is a group of events in which microphonic noises were so large that the baseline went out of the input range of the FADCs. They are distinguished by their waveforms and the live time was estimated after the most conservative manner. No correction is needed for cut (b) which is also aimed at cosmic-ray events, since the expected rate of the axion events is extremely low. Cut (c) and (d) were introduced to simplify

the later waveform analysis. The loss in efficiency by cut (c) was found to be negligible. The causes of the slow pulses may be some kind of spontaneous noises of the detector, but are yet to be identified. However, it was confirmed that they were at least not X-rays, since we could hardly find such events in the data in which the ^{55}Fe source was observed. In order to estimate the loss in efficiency by cut (d), the same cut was applied to the ^{55}Fe source data. We found it to be less than 2.6% using the worst value of the sixteen channels.

We performed numerical pulse shaping to the raw waveforms using the Wiener filter. The energy of an X-ray is given by the peak height of a wave after shaping. The shaped waveform is given by

$$U(\omega) = \frac{S^*(\omega)C(\omega)}{|N(\omega)|^2}, \quad (4)$$

where $U(\omega)$, $S(\omega)$, $C(\omega)$, and $N(\omega)$ are Fourier transformations of the shaped waveform, the ideal signal waveform, the measured waveform, and the noise, respectively. Noises are obtained by gathering waveforms while no trigger exists, and the ideal signal waveform is approximated by averaging signals from 5.9-keV X-rays. The response function of this waveform analysis, i.e., non-linearity, gain walk by trigger timing, etc., was investigated thoroughly using simulated pulses which were obtained by adding the template waveform to the noise waveforms. A correction was made based on this numerical simulation. Saturation arised at about 25 keV, therefore, $E > 20$ keV was not used in the later analysis. Fig. 3 shows the comprehensive background spectrum of all the photodiodes and all the gas settings. The background level was about $1.5 \times 10^{-5} \text{s}^{-1} \text{keV}^{-1} / \text{PIN}$ at $E = 5\text{--}10$ keV. The peak appearing at 22 keV is consistent with the fluorescent X-rays from the small amount of silver epoxy between the photodiode chip and the Kapton base. By analysing the calibration data, we found the energy resolution of each photodiode to be 0.70–0.87 keV (FWHM) for 5.9-keV photons.

In Fig. 4, one of the energy spectra of the solar observation is shown together with the background spectrum. We searched for expected axion signals which scale with $g_{a\gamma\gamma}^4$ for various m_a in these spectra. The smooth curve in the figure represents an example for the expected axion signal where $m_a = m_\gamma = 0.263$ eV and $g_{a\gamma\gamma} = 7.4 \times 10^{-10} \text{GeV}^{-1}$, which corresponds to the upper limit at $m_a = 0.263$ eV estimated as follows.

A series of least χ^2 fittings was performed assuming various m_a values. Data from the ten different gas densities were combined by using the summed χ^2 of the ten. The energy region of 4–20 keV was used for fitting where the efficiency of the trigger system is almost 100% and the FADCs do not saturate. The PIN photodiodes were assumed to have inactive surface layers of $6.1 \mu\text{m}$ [11]. As a result, no significant excess was seen for any m_a , and thus an upper limit on

$g_{a\gamma\gamma}$ at 95% confidence level was given following the Bayesian scheme. Fig. 5 shows the limit plotted as a function of m_a . The previous limit and some other bounds are also plotted in the same figure. The SOLAX [14] is a solar axion experiment which exploits the coherent conversion on the crystalline planes in a germanium detector. The COSME [15] is the same kind of experiment but with a different Ge detector at a different site. Though their limits $g_{a\gamma\gamma} < 2.7 \times 10^{-9}\text{GeV}^{-1}$ and $g_{a\gamma\gamma} < 2.78 \times 10^{-9}\text{GeV}^{-1}$, respectively, are loose, they are virtually independent of m_a like the following two theoretical bounds. It is also worth noting that they are observational. The limit $g_{a\gamma\gamma} < 2.3 \times 10^{-9}\text{GeV}^{-1}$ is the solar limit inferred from the solar age consideration and the limit $g_{a\gamma\gamma} < 1 \times 10^{-9}\text{GeV}^{-1}$ is a more stringent limit reported by Schlattl et al. [16] based on comparison between the helioseismological sound-speed profile and the standard solar evolution models with energy losses by solar axions.

4 Discussion and Conclusion

We have developed an axion helioscope and introduced cold helium gas as the dispersion-matching medium in the $4\text{T} \times 2.3\text{m}$ magnetic field of the helioscope. The axion mass up to 0.27eV has been scanned. But no evidence for solar axions was seen. A new limit on $g_{a\gamma\gamma}$ shown in Fig. 5 was set for $0.05 < m_a < 0.27\text{eV}$, which is far more stringent than the solar-age limit. This experiment could also clear some area beyond the tighter helioseismological bound. This limit assumes the standard solar model by Eq. 1, and depends especially on the core temperature. Though the limit did not reach the preferred axion models, this experiment is currently the only experiment which has demonstrated enough sensitivity to detect such solar axions that do not violate these solar limits.

The exact position of the ‘hadronic axion window’ or whether it is still open or not are controversial [19,20]. There is an argument that it has closed by the globular-cluster limit [18]. As for the solar limits, Watanabe and Shibahashi [17] has recently argued that the helioseismological bound can be lowered to $g_{a\gamma\gamma} < 4.0 \times 10^{-10}\text{GeV}^{-1}$ if the ‘seismic solar model’ and the observed solar neutrino flux are combined. Discussions based on mutually independent assumptions are meaningful. And, it must be essential to test by well-controlled experiments or by direct observations. We are planning to upgrade our helioscope to scan higher masses. The CAST experiment [21] at CERN aims sensitivity as high as $g_{a\gamma\gamma} \approx 5 \times 10^{-11}\text{GeV}^{-1}$.

Acknowledgements

The authors thank the director general of KEK, Professor H. Sugawara, for his support in the beginning of the helioscope experiment. This research is supported by the Grant-in-Aid for COE research by the Japanese Ministry of Education, Science, Sports and Culture, and also by the Matsuo Foundation.

References

- [1] R.D. Peccei, H.R. Quinn, *Phys. Rev. Lett.* 38 (1977) 1440.
- [2] R.D. Peccei, H.R. Quinn, *Phys. Rev. D* 16 (1977) 1791.
- [3] S. Weinberg, *Phys. Rev. Lett.* 40 (1978) 223.
- [4] F. Wilczek, *Phys. Rev. Lett.* 40 (1978) 279.
- [5] J.E. Kim, *Phys. Rep.* 150 (1987) 1.
- [6] M.S. Turner, *Phys. Rep.* 198 (1990) 67.
- [7] L.J Rosenberg, K. van Bibber, *Phys. Rep.* 325 (2000) 1.
- [8] G.G. Raffelt, *Phys. Rep.* 333–334 (2000) 593.
- [9] P. Sikivie, *Phys. Rev. Lett.* 51 (1983) 1415.
- [10] K. van Bibber et al., *Phys. Rev. D* 39 (1989) 2089.
- [11] S. Moriyama et al., *Phys. Lett. B* 434 (1998) 147.
- [12] T. Namba et al., astro-ph/0109041, to be published in *Nucl. Instr. Meth. A*.
- [13] G. H. Kaplan et al., *Astronomical Journal* 97 (1989) 1197;
URL: <http://aa.usno.navy.mil/AA/software/novas/>.
- [14] A.O. Gattone et al., *Nucl. Phys. B (Proc. Suppl.)* 70 (1999) 59.
- [15] A. Morales et al., *Astropart. Phys.* 16 (2002) 325.
- [16] H. Schlattl, A. Weiss, G. Raffelt, *Astropart. Phys.* 10 (1999) 353.
- [17] S. Watanabe, H. Shibahashi, hep-ph/0112012.
- [18] G. G. Raffelt, *Stars as Laboratories for Fundamental Physics*, (The University of Chicago Press, 1996).
- [19] P. Astier et al., *Phys. Lett. B* 479 (2000) 371.
- [20] J. Hisano, K. Tobe, T. Yanagida, *Phys. Rev. D* (1997) 411.
- [21] K. Zioutas et al., *Nucl. Instr. Meth. A* 425 (1999) 480.

- [22] Y. Sato et al., Development of a Cryogen-free Superconducting Dipole Magnet, in: Proc. of the 15th International Conference on Magnet Technology (MT-15) (Beijing, October 1997), eds.: L. Liangzhen, S. Guoliao, Y. Luguang (Science Press, Beijing, 1998) pp. 262–265; KEK-Preprint-97-202 (November, 1997).
- [23] Vincent D. Arp and Robert D. McCarty, Thermophysical Properties of Helium-4 from 0.8 to 1500 K with Pressures to 2000 MPa, NIST Technical Note 1334, (U.S. Department of Commerce, National Technical Information Service, 1989).

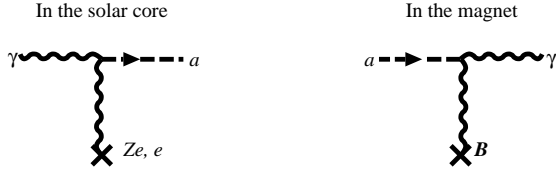


Fig. 1. The solar axions produced via the Primakoff process in the solar core are, then, converted into X-rays via the reverse process in the magnet.

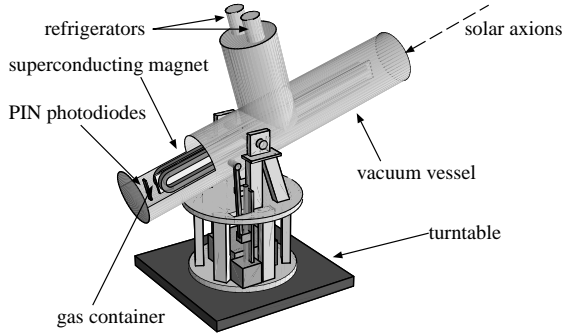


Fig. 2. The schematic view of the axion helioscope.

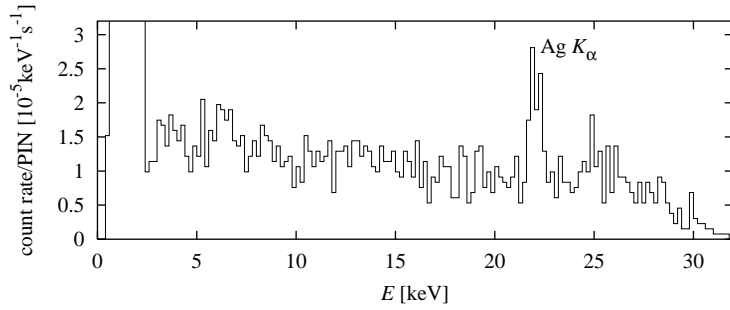


Fig. 3. The background spectrum of the X-ray detector. The sixteen PIN photodiodes and the ten gas densities are combined.

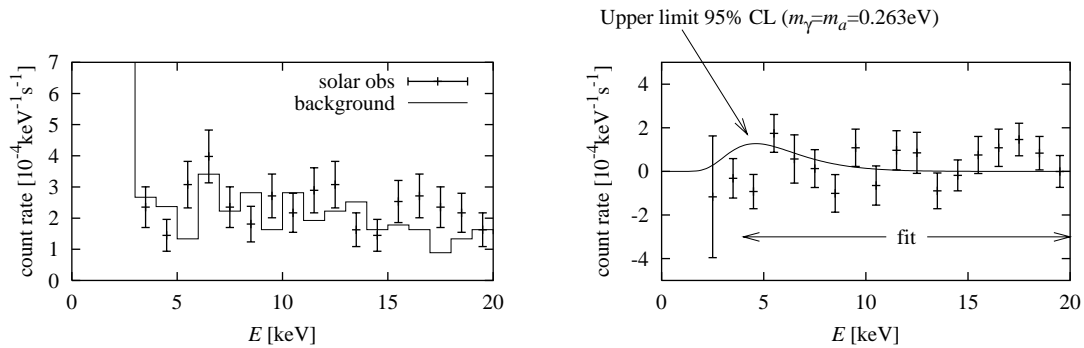


Fig. 4. The left figure shows the energy spectrum of the solar observation (error bars) and the background spectrum (solid line) when the gas density was tuned to $m_\gamma = 0.263\text{eV}$. The right figure shows the net energy spectrum of the left where the background is subtracted from the solar observation.

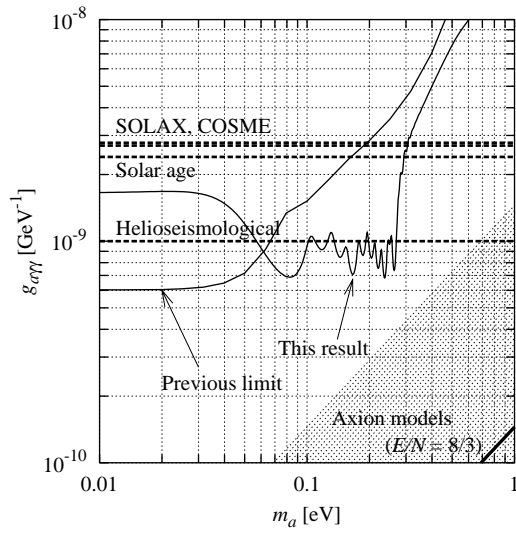


Fig. 5. The exclusion plot on $g_{a\gamma\gamma}$ to m_a is plotted where some other bounds are plotted together. The new limit and the previous one are plotted in solid lines. Dashed lines are the limit by SOLAX experiment, the limit by COSME experiment, the limit inferred from the solar age consideration, and the helioseismological bound. The four observational limits are at 95% confidence level. The hatched area is the preferred axion models. The thick line corresponds to the case when a simple GUT is assumed.

molar density [mol/m ³]	m_γ [eV]	live time [s]	
		solar run	background
4.137	0.083	26245	35955
8.325	0.118	25866	34606
12.52	0.144	26111	35383
16.62	0.166	23088	34399
20.80	0.186	24876	35161
25.15	0.204	38355	50701
29.19	0.220	25478	35411
33.70	0.237	40356	51989
37.58	0.250	12638	30216
41.65	0.263	55289	67443

Table 1
Table of the gas settings and each live time.